



FRACTURE PROPERTIES OF LOCAL ASPALT CONCRETE

HAMED M. H. AL-HAMDOU

Professor Emeritus

Civil Eng. Dept./Eng. College/Baghdad University

e mail: profhamedalani@yahoo.com

Dr. ABDUL-HAQ HADI ABED-ALI

Assistant Professor

Highways & Transportation Dept./Eng. College

Al-Mustansiriyah University

e mail: abdulhaq-alhaddad@yahoo.com

Dr. MOHAMMED Z. MOHAMEDMEKI

Lecturer

Highways & Transportation Dept./Eng. College

Al-Mustansiriyah University

e mail: moh7312@gmail.com

ABSTRACT

The local asphalt concrete fracture properties represented by the fracture energy, J-integral, and stress intensity factor are calculated from the results of the three point bending beam test made for pre notches beams specimens with deformation rate of 1.27 mm/min . The results revealed that the stress intensity factor has increased by more than 40% when decreasing the testing temperature 10°C and increasing the notch depth from 5 to 30 mm . The change of asphalt type and content have a limited effect of less than 6%.

Key words: Stress intensity factor, Fracture Energy, J-integral

خواص الكسر للخرسانة الاسفلتية المحلية

حامد محمود حمدو

استاذ مشارك

قسم الهندسة المدنية / كلية الهندسة / جامعة بغداد

د. محمد زهير محمد مكي

مدرس

قسم هندسة الطرق / كلية الهندسة / الجامعة المستنصرية

د. عبد الحق هادي عبد علي

استاذ مساعد

قسم هندسة الطرق / كلية الهندسة / الجامعة المستنصرية

الخلاصة

خلال هذه البحث تم دراسة خصائص التصدع للخرسانة الاسفلتية المحلية المتمثلة بطاقة التصدع؛ J-Integral و معامل شدة الاجهاد والتي تم احتسابها لنماذج العتبات المسبقة الشق من خلال فحصها باستخدام فحص الانثناء وبسرعة تشوه مقدارها 1.27 mm/min . اوضحت الدراسة بان معامل شدة الاجهاد قد ارتفع اكثر من 40% بخفض درجة حرارة الفحص 10 درجات مئوية وبزيادة عمق الشق المسبق (pre notch) من 5 mm الى 30 mm بينما كان لتغييرنسبة ونوع الاسفلت تأثير محدود لم يتجاوز 6%.

1. INTRODUCTION

Cracking is one of the major distresses in flexible pavement, results from exposure of pavement structure to environmental conditions and traffic loading. Accurate prediction of crack initiation and propagation aids in the design and maintenance of asphalt pavement structures. Crack initiation and its relation with material mechanical behavior can be used to describe the remaining service life of the existing pavements. Several test methods were developed to study the cracking behavior in Hot Mix Asphalt (HMA) under different sample geometries, loading configurations, and material properties **Denneman, et. al., 2009, Im, 2012**. In most tests, a notch was introduced into the sample so that the crack would initiate at the notch **Kim, and El Hussein, 1995**. In many of these studies, linear elastic fracture mechanics and elastic plastic fracture mechanics principles were applied to characterize material response.

2. FRACTURE MECHANICS

Fracture mechanics is the material mechanical behavior when subjected to load in the presence of cracks; in other words, it is the stress/strain characteristics of the pre-cracked material subjected to load or deformation **Saadeh, and Hakimelahi, 2012**.

2.1 Crack modes

Generally, there are three crack modes; these modes depend on the crack nature of cracked bodies. **Fig.1** shows these modes and a short description for each one is given below **Saxena, 1998**:

Mode I: Opening mode, the crack surfaces separate symmetrically with respect to X-Y and X-Z planes.

Mode II: Sliding mode, the crack surfaces relatively slide to each other symmetrically with respect to X-Y plane and symmetrically skew with respect to X-Z plane.

Mode III: Tearing mode, the crack surfaces relatively slide to each other symmetrically with respect to X-Y and X-Z planes.

For the purpose of this research, *mode I (Opening mode)* is adopted because it mostly represents the nature of pavement structure crack as shown in the **Fig.2**. Furthermore, widely accepted theories for fracture under mode II, III, and mixed mode conditions are currently not available **Saxena, 1998**.

2.2 Stress Intensity Factor

The stress intensity factor (K) represents the amplitude of the crack tip stress singularity and is dependent on body geometry, crack size, load level, and loading configuration. The **Eq.(1)** of estimating the (K) is:

$$K = \frac{P}{BW^{1/2}} F(a/W) \quad (1)$$

Where: *P*: Reaction point load,
B: Specimen thickness,
W: Specimen depth,
a: Crack length, and



$F(a/W)$: Dimensionless calibration functions for various geometries, as shown in **Table 1** as reported by **Saxena, 1998**.

2.3 The J-Integral Approach

In 1968, Rice, published papers in which he discussed the potential of a path-independent integral (J) for characterizing fracture in nonlinear-elastic materials **ASM, 1997**. This integral is identical in form to the static component of the energy moment tensor for characterizing generalized forces on dislocations and point defects introduced by Eshelby G.P. Cherapov, working independently in the former Soviet Union during the same time of Rice. Cherapov, 1967 also presented a formulation of an integral similar to Rice's (J). Rice defined the J-Integral for a cracked body, shown in **Fig.3**, as follows in **Eq. (2 and 3)**:

$$J = \int_S (Ws.n - T \partial ui / \partial x) ds \tag{2}$$

$$J = \int_S Ws.dy - T \partial ui / \partial x . ds \tag{3}$$

Where: Ws : elastic strain energy,

T : Traction vector defined according to the out word normal n the contour S , and

u : Displacement vector ($u1i + u2j$).

J can be shown to relate to the rate of changes of potential energy with respect to change in crack size. This interpretation of J is useful in showing that under linear elastic condition, $J=Y$ **Eq.(4)**:

$$U = \int_A W(X,Y) dA - \int_S Ti ui ds \tag{4}$$

Where: A : Body area, Ti : Traction, and ui : Displacement. } applied along the boundary

by differentiating the previous equation get **Eq.(5)**:

$$\frac{dU}{da} = \int_A \frac{dW}{da} dA - \int_S Ti \frac{d ui}{da} ds \tag{5}$$

The contour of the line integral can be extended along the boundary S of the body in the counterclockwise direction from the lower crack face to the upper one, since $\frac{dU}{da} = 0$, on the boundary S_u , the displacements are prescribed independently of a , as shown in **Fig.4**.

By substituting the coordinate system attached to the crack tip, and using the symmetry of the stress tensor with the application of the divergence theorem, the equation becomes as shown in **Eq. (6 and 7)**:

$$\frac{dU}{da} = - \int_S W dy - \int_S Ti \frac{\partial ui}{\partial x} ds \tag{6}$$

For unit thickness body $J = - \frac{dU}{da}$ } **(7)**
 For a body with thickness (B) $J = - \frac{1}{B} \frac{dU}{da}$ }

Under certain restriction, J can be used as an elastic-plastic energy release rate. The path independence of J -integral expression allows calculation along a contour remote from the crack tip; such a contour can be chosen to contain only elastic loads and displacements. Thus, an elastic-plastic energy release rate can be obtained from an elastic calculation along a contour for which loads and displacements are known. In 1972, Begley, J. A. and Landes, J. D. **ASM, 1997** developed an experimental method for determining J from generating load-displacement curves for samples of unit thickness with different initial crack lengths.

3. ASPHALT CONCRETE FRACTURE

Uzan, and Levenberg, 2001 studied the phenomenology of asphalt concrete (AC) fracture in the laboratory under uniaxial-tension with strain control of $0.6^{\text{mm}/\text{min}}$ at the room temperature of 24°C for beam samples of about $(60 \times 90 \times 225^{\text{mm}})$. The study showed that the pre-peak stress conditions induced damage is a result of formation, growth and coalescence of micro cracks; the study also found in post-peak stress condition that the process of damage localization occurs within the Representation Volume Element (RVE) (the zone across the sample of 2-4 times their nominal maximum size of mix aggregate Witczak, 2000 at which the crack will propagate) leading to the creation of a dominant failure surface and eventually fracture. The study added that the cracking behavior of an AC MIX of RVE size, three scales of load induced cracks should be considered as shown in **Fig.5**:

1. Micro-cracks: small flows up to few millimeters (the air voids entrapped during compaction process may represent these flows).
2. Meso-cracks: resulting from micro cracks coalescence; their length may reach the maximum aggregate size in the mix.
3. Macro-cracks: at which the strength of AC is reduced to zero and of a minimal RVE in size.

Kim, et. al. 2008 used a bilinear cohesive softening model to simulate the crack initiation and propagation in asphalt concrete. The meso-crack representation of material morphology was incorporated into the model using high-resolution imaging.

Kim and co-researchers explained the bilinear cohesive softening model concept as follows and as shown in **Fig.6**. In general the cracking of asphalt concrete can occur in any weak point within the fracture process zone **Fig.6-a** and cohesive fracture concept at the crack tip can be simplified as shown in **Fig.6-b**. In **Fig.6**, σ_{max} represents the location of cohesive crack tip and δ_{sep} is the complete material separation or the material crack tip, and σ_{max} is the normal cohesive strength. Point B represents the starting point of unrecoverable material degradation (or micro-crack initiation) and point c represents the condition where a crack face was fully separated and released the energy potential associated with losing of cohesive strength.

In **2008** at Cambridge University UK, **Portillo and Cebon** investigated the fracture mechanics of idealized asphalt mix (bitumen of penetration grade of 40-50 and fraction of sub spherical sand between $150\text{-}300^{\mu\text{m}}$) using a systematic 3-point bending test for beam samples of $(50 \times 50 \times 225^{\text{mm}})$ with middle notch of length equal to half of depth, in order to develop fracture mechanism maps classifying the brittle, ductile, and transition response of the materials as a function of temperature and load rate. The experimental data of this study was analyzed in terms of stress intensity factor, fracture energy, and J -integral at the temperature range of -30°C to 30°C with two deformation rate of 0.01 and $0.05^{\text{mm}/\text{sec}}$.

The study showed that, for typical force vs. deflection curves, the peak force increases with temperature; at 0°C , the crack arrests in the vicinity of peak load and the crack grows in a smooth fashion a more brittle behavior and less energy is required to propagate the crack. **Fig.7** shows the

typical load line displacement curve for tested sample at -20°C with displacement rate of 0.05mm/sec made by this study.

3.1 Materials

For the purpose of this study, two types of local asphalt cement, obtained from AL-Daurah refinery, including 40-50 and 60-70 penetration graded and quartzite crushed aggregates were selected to be used in this study. The crushed aggregates were obtained from AL-Nebai quarry, due to the extensive usage of this type of aggregates for asphaltic mixtures in the middle of Iraq especially in Baghdad city. The limestone dust, from Karbala governorate, was used as a filler material.

The main properties of selected materials for the purpose of this research, which include two types of asphalt cement, quartzite crushed aggregates and limestone dust as mineral filler, are presented in the following **Tables 2 to 6**.

3.2 Mix design and optimum binder content determination

For the purpose of this study the Hot Mix Asphalt concrete (HMA) was designed volumetrically according to the SUPERPAVE requirements, the aggregates gradation was selected to meet the Iraqi specification beside the SUPERPAVE to be as shown in the gradation curve presented in **Fig.8** with 0.5^{in} as a maximum nominal aggregate size representing wearing layer.

Based on the results of rotational viscometer (ASTM D4402, AASHTO T316) the HMA was mixed and compacted at the required equiviscous temperatures shown in **Table 7**.

The HMA was compacted by using the gyratory compactor (ASTM D6925-09, AASHTO T312) after aging period of 4 hours @ 135°C with 8,100, and 160 as a number of gyration initial, designed, and maximum respectively as presented in **Table 8** to meet the mix design subjected to number of equivalent axels to be passed on pavement during its design life which used here between 3.0 to 30.0 million ESALs.

The results of volumetric properties represented by Air Voids, Voids in Mineral Aggregates (VMA), and Voids Filled with Asphalt (VFA) for the gyratory compacted specimens shown on the **plate 1** are fitted with asphalt content and the Optimum Binder Content (OBC) of 4.7% is found to get the required properties as needed by SUPERPAVE criteria as shown in **Table 9**, it is worth to mentioned here that there is no significant difference is found on OBC between asphalt penetration graded 40-50 and 60-70.

3.3 Study parameters

The following parameters are considered at this study

- Two testing temperature 20°C and 30°C ,
- Three pre crack depth (notch) 5, 15, and 30^{mm} ,
- Two asphalt type 40-50 and 60-70 penetration graded, and
- Three asphalt content, optimum and $\pm 0.5\%$.

So, and according to these parameters the required specimens number are 36 beams which prepared as describe in the following section.

3.4 Specimens preparation

In order to study the fracture properties of HMA subjected to bending stress beams specimens of $3 \times 3 \text{in}$ ($7.62 \times 7.62^{\text{cm}}$) cross section and 15^{in} (38.1^{cm}) length with gross mass of about 5150gm were made with different notch depth. A steel rectangular mold of (15^{in} length X 4^{in} depth X 3^{in} width) ($38.1 \times 10 \times 7.62^{\text{cm}}$) inside dimensions with two spacers made by **Fadthl, 2007**, is used for producing beams specimens as shown in **Plate 2**.

The specimens were compacted by using the uniaxial digital compression machine having a capacity of 2000^{kN} as shown in **Plate 2**, to get the required air voids (4%±1% for wearing layer) for specimens with different asphalt content; the relations between applied stress and %G_{mm} were made as shown in **Fig.10**, so from these relations, the required applied stress was found for mixes of different asphalt content as presented in the same figure.

A steel plate of (3^{mm} thickness) which welded perpendicularly on base plate of (6^{mm} thickness) were used to make a notch on the specimens by placing it in the mold before applying the mix in the mold and then by removing it after the completion of the compaction process. To make a different notch depth, three plates arrangements were used with different perpendicular plate height of (5, 15, and 30^{mm}) as shown in **Plate 3**.

3.5 Testing

A load frame device, manufactured by Humboldt company in the USA model HM-2800, with digital control unit for multi deformations rates (ranging from 0.001(0.0254) to 2^{in/min} (50.8^{mm/min})) was used to test the specimens monotonically in order to generate the Load- Displacement (L-D) curves for tested specimens. Some modifications were made on device as shown in **Plate 4**, by adding load cell and fully isolated chamber made with aluminum frame and sandwich panel of 5^{cm} thickness and double glasses door in addition to that heating and cooling sources were provided with thermometer sensor and digital thermostat to maintain the specified temperature during the test.

3.6 Bending Beam Test (BBT) fracture energy and J-Integral

In order to specify the fracture properties of local asphalt concrete, the value of J-integral was estimated using the experimental method. As pointed in Chapter Two, J-integral was defined and shown to characterize the process of ductile tearing under elastic-plastic and fully plastic conditions. Further, its magnitude should be easily measurable in test specimens used for characterizing crack growth resistance.

Experimental method which was developed by J.A. Begley and J.D. Lands in 1972 needs to generate Load-Displacement (L-D) for specimens of unit thickness with different initial crack lengths. Each specimen is loaded to displacement levels that can be sustained without crack extension. The areas under load displacement curves to specified values of displacement D1, D2, D3, ... Di are obtained graphically to determine the corresponding values of the potential energy U1, U2, U3, ... Ui. For each fixed value of displacement, Ui can be plotted as a function of crack length ai. The slope of U-a curve, dU/da, is then measured at various points to yield the values of J. If the specimen thickness is other than unity, dU/da must be divided by the thickness, B, in order to obtain the value of J. The resulting J values can be plotted as a function of the applied displacement for various crack size **Saxena, 1998**.

The fracture properties were estimated by generating the Load-Displacement (L-D) curves for beams specimens made as explained in the previous chapter with initial cracks (notches) of 5, 15, and 30^{mm} lengths. A three point BBT test was made by using digital load frame device, as shown in **Plate 4**, with deformation rate of 0.05^{in/min} (1.27^{mm/min}). The specimens reaction load was indicated by employing a load cell of 5.0^{kN} capacity; the load reaction history was recorded by using a digital camera which faced to the load cell reader.

Figers 11-a to c show the application of experimental method explained earlier to estimate the fracture properties which include fracture energy and J-integral; the load displacement curves were divided into two parts: pre peak and post peak.

The pre peak part represents the tested specimen before cracks initiate. This part is divided to segments as shown in **Fig. 11-a** of 0.75^{mm} at horizontal axis which represent the displacement;

then the areas under the curves were calculated through integrating the polynomial equations of each curves at incremental value of 0.75^{mm} until 3mm and then the relation was made between the fracture energy and crack length as shown in **Fig. 11-b**. The slopes were found for previous relations and the values of J-integrals were calculated and the relations between J-integrals and displacement were made for different notch depths as shown in **Fig. 11-c**. **Figures 11-a, b, and c** illustrate the results of tests which were made for beams specimens made with asphalt cement of 40-50 penetration graded at optimum binder content tested at 20±1°C; while **Figures 12-a, b, and c** show the results of the same tests but at 30±1°C.

3.7 Stress intensity factor

The stress intensity factor (K) represents the amplitude of the crack tip stress singularity and is dependent on body geometry, crack size, load level, and loading configuration. The **Eq.1** presented in section of stress intensity factor is used here to calculate the magnitude of (K) for beams specimens as shown below:

$F(a/W)$ = dimensionless calibration functions for various geometries and different notch depth as given in **Eq.8**:

$$F(a/W) = \frac{3\left(\frac{S}{W}\right)\left(\frac{a}{W}\right)^{\frac{1}{2}}\left[1.99 - \frac{a}{W}\left(1 - \frac{a}{W}\right)\left(2.15 - 3.93\left(\frac{a}{W}\right) + 2.7\left(\frac{a}{W}\right)^2\right)\right]}{2\left(1 + \frac{2a}{W}\right)\left(1 - \frac{a}{W}\right)^{3/2}} \quad (8)$$

where:

S : clear span =4W (12"), see **Table 1**.

So, the calibration function for studied notch depths are calculated and illustrated in **Table10**. Accordingly and by using **Eq.1**, the magnitudes of stress intensity factor was calculated for beams specimens and it was found that the (K) value increased with increasing notch depth, due to increasing crack length which means reducing the depth to the crack tip and increasing the stress concentration for the same applied load. In other words, the load required to bend and crack the specimen is decreased with increasing the crack length. **Fig.13** shows the effect of notch depth on stress intensity factor for beams specimens tested at 20±1°C and 30±1°C; based on this figure, the effect of notch depth is decreased when raising the test temperature.

4. SENSITIVITY ANALYSIS

The effect of study parameters on stress intensity factor are shown and discussed at following sections

4.1. Notch depth

Three notch depths (5, 15, and 30^{mm}) were made for beam specimens tested monotonically with constant deformation rate of 0.05^{in/min}, at two testing temperatures 20±1°C and 30±1°C; the effect of notch depths on the stress intensity factor was illustrated in **Fig.14**.

The figure gives an idea about the effect of notch depths on the stress concentration at the crack tip, as the notch depth increase the stress concentration increased; that explained the rapid deterioration of asphalt concrete section having cracks if compared with non cracked section.

4.2. Testing Temperatures

When raising the testing temperature from 20±1°C to 30±1°C, the behavior of asphalt concrete changed from brittle material to plastic material and that led to reducing the stress intensity factor and increasing deformation before cracking initiation. The reduction increases with increasing



notch depth due to decreasing the load required to bend and break the specimens with increasing testing temperature. **Fig.15** shows the effect of testing temperature on the stress intensity factor for the tested beam specimens of different notch depths.

4.3. Asphalt Type

It was found that the asphalt type has no significant effect on the stress intensity factor for the tested specimens especially at low testing temperature at which the effect did not exceed 1% for 5^{mm} notch depth; when rising the testing temperature, the effect increased to be about 3% for the same notch depth. The stress intensity factor reduced slightly when changing the asphalt type from 40-50 to 60-70 penetration graded because the asphalt 40-50 is harder than 60-70 and that led to decreasing the load required to bend and break the beam specimens made with asphalt type of 60-70 penetration graded. **Fig.16** shows the effect of asphalt type on stress intensity factor of tested beam specimens of different notch depths.

4.4. Asphalt Content

The effect of asphalt content on stress intensity factor increased with decreasing the notch depth which was ranging from $\pm 0.5\%$ to $\pm 2\%$ at $20 \pm 1^\circ\text{C}$ testing temperature and from $\pm 1.5\%$ to $\pm 6\%$ at $30 \pm 1^\circ\text{C}$ testing temperature as presented in **Figures 17** and **18**. The stresses concentration decreased when decreasing the asphalt content due to decreasing the cementing material and increasing the air voids which form a discontinuity points in the mix that led to decreasing the load needed to bending and breaking the beam specimens.

5. CONCLUSION

From the results of this study it can be concluded that the fracture properties of asphalt concrete are mainly affected by decrease the temperature and presence of cracks that increase the stress concentration at the crack tip. The decrease in temperature causes the asphaltic material to become harder with low ductility and brittle behavior under the effect of traffic wheel loads. The presence of crack decreases the effective pavement depth that can resist the crack propagation. More deterioration is expected in pavement section with high flaws, which necessitate an early preventive maintenance. The sensitivity of stress intensity factor for the various study parameters, is shown in **Table 11**.

REFERENCES

- American Association of State Highway and Transportation Officials AASHTO ,1993,"*Guide for Design of Pavement Structures*" Washington, D. C., USA.
- American Association of State Highway and Transportation Officials AASHTO ,2010,"*Standard Specifications for Transportation Materials and Methods of Sampling and Testing*" , Washington, D. C., USA.
- American Society of Metals ASM ,1997, "*Fatigue and Fracture*" Handbook, Volume 19, 2nd Printing, USA.



- American Society for Testing and Materials ASTM ,2009, "*Road and Paving Materials*" Annual Book of ASTM Standards, Volume 04.03, West Conshohocken, USA.
- Asphalt Institute ,2003, "*Performance Grade Asphalt Binder Specification and Testing*" Manual Series No.2, SP-2, Lexington, Kentucky.
- Denneman, E., R. Wu, E.P. Kearsley, and A.T. Visser, 2009, "*Fracture Mechanics in Pavement Design*" Proceedings of the 28th Southern African Transport Conference, PP. 255-262, 6-9July.
- Fadhel, T. H., 2007, "*Some Requirements to Control Reflective Cracking of Overlay Asphalt Pavement*" Ph.D. Thesis, Civil Engineering Department, College of Engineering, University of Baghdad.
- Im S. , 2012, "*Characterization of viscoelastic and fracture properties of asphaltic materials in multiple length scales*", Ph. D thesis, University of Nebraska, May.
- Kim, H., W.G. Buttler, M.N. Partl, 2008,"*Investigation of Fracture Toughening Mechanisms of Asphalt Concrete Using the Clustered Discrete Element Method*" Proceeding of the 8th Swiss Transport Research Conference, Monte Verita / Ascona, October 15-17.
- Kim, K.W., and H.M. El Hussein, 1995, "*Effect of Differential Thermal Contraction on Fracture Toughness of Asphalt Materials at Low Temperatures*" Proceeding of the Association of Asphalt Paving Technologists, volume 64, Portland, Oregon, March 27-29.
- Perng, J. , 1989, "*Analysis of Crack Propagation in Asphalt Concrete Using a Cohesive Crack Model*" MS c. thesis, Ohio State University.
- Portillo, O. and D. Cebon, 2008, "*An Experimental Investigation of the Fracture Mechanics of Bitumen and Asphalt*" Proceeding of the 6th Rilem International Conference on Cracking in Pavements, Chicago, USA, 16-18 June, PP. 627-636.
- Saadeh, S. and Hakimelahi, H. , 1998, "Investigation of Fracture Properties of California Asphalt Concrete Mixtures" Project No. 11-21,California state university long beach, department of civil engineering and construction engineering management, September, 2012.
- Saxena, A. "*Nonlinear Fracture Mechanics for Engineers*" CRC Press LLC, USA.
- State Corporation of Roads and Bridges SCRБ, 2003, "*General Specification for Roads and Bridges/ Section R9, Hot Mix Asphalt Concrete Pavements*" Revised Edition, Ministry of Housing and Construction, Republic of Iraq.
- Uzan, J. and E. Levenberg , 2001,"*Strain Measurements in Asphalt Concrete Specimens towards the Development of a Fracture Model*" International Journal Pavement Engineering, Volume 2(4), PP. 243-258, Overseas Publishers Association OPA.

**NOMENCLATURE**

- P*: Reaction point load
B: Specimen thickness
W: Specimen depth
a: Crack length
F(a/W): Dimensionless calibration functions for various geometries
Ws: elastic strain energy
T: Traction vector defined according to the outward normal *n* the contour *S*
u: Displacement vector ($u_1i + u_2j$)
A: Body area,
T_i: Traction, and
u_i: Displacement.
S: Clear span = 4W (12")

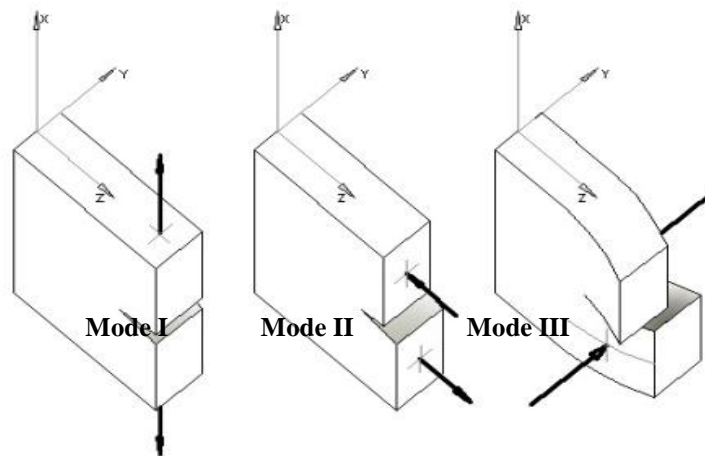


Figure 1. Crack modes, Saxena, 1998.

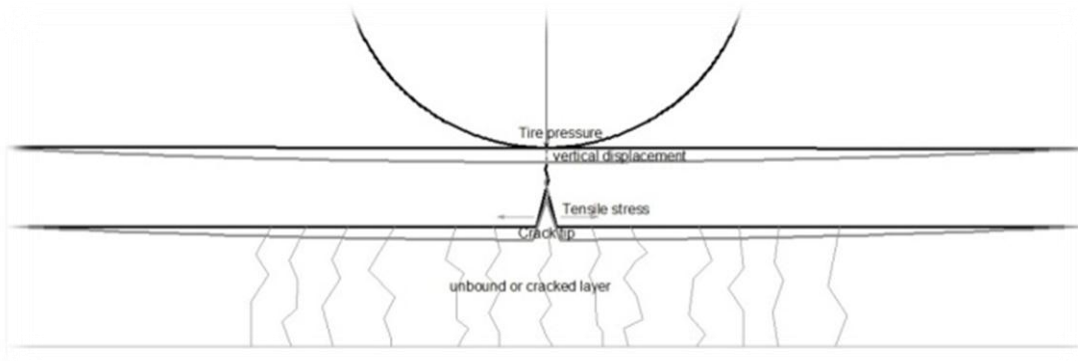
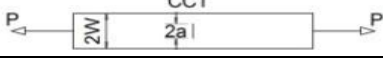
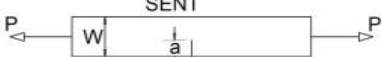
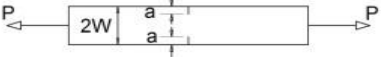
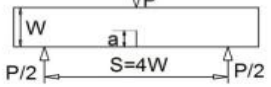


Figure 2. Crack in pavement.

Table 1. Dimensionless calibration functions for various geometries Saxena, 1998.

Geometry	$F(a/W)$
Center Crack Tension CCT 	$\frac{1}{2} \sqrt{\pi \frac{a}{W} \sec \frac{\pi}{2} \left(\frac{a}{W}\right)} \left[1 - .25 \left(\frac{a}{W}\right)^2 + 0.06 \left(\frac{a}{W}\right)^4 \right]$
Single Edge Notch Tension SENT 	$\frac{\left(2 \tan \frac{\pi a}{2W}\right)^{1/2}}{\cos \frac{\pi a}{2W}} \left[0.752 + 2.02 \left(\frac{a}{W}\right) + 0.37 \left(1 - \sin \frac{\pi a}{2W}\right)^3 \right]$

<p>Double Edge Notch Tension DENT</p> 	$\frac{\frac{1}{2} \left(\frac{\pi a}{W}\right)^{1/2}}{\left(1 - \frac{a}{W}\right)^{1/2}} \left[1.122 - 0.561 \left(\frac{a}{W}\right) - 0.205 \left(\frac{a}{W}\right)^2 + 0.471 \left(\frac{a}{W}\right)^3 - 0.19 \left(\frac{a}{W}\right)^4 \right]$
<p>Single Edge Notch Bending SENB</p> 	$\frac{3 \left(\frac{S}{W}\right) \left(\frac{a}{W}\right)^{1/2} \left[1.99 - \frac{a}{W} \left(1 - \frac{a}{W}\right) \left(2.15 - 3.93 \left(\frac{a}{W}\right) \right) + 2.7 \left(\frac{a}{W}\right)^2 \right]}{2 \left(1 + \frac{2a}{W}\right) \left(1 - \frac{a}{W}\right)^{3/2}}$

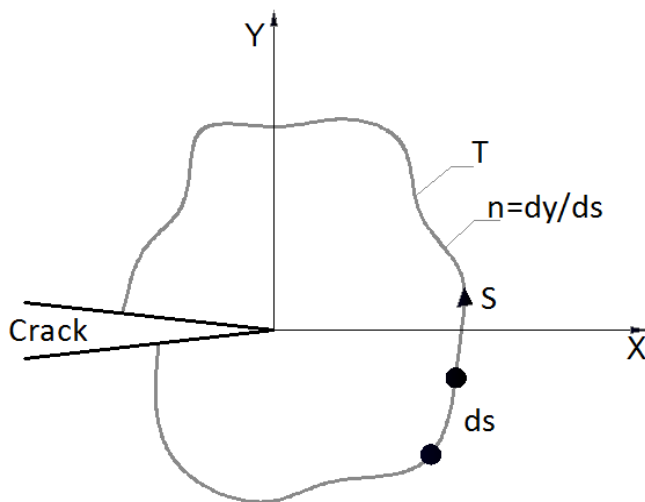


Figure 3. A 2-dimensional cracked body with a contour S originating from the lower cracked surface and going counterclockwise terminating at the upper crack surface, **Saxena, 1998.**

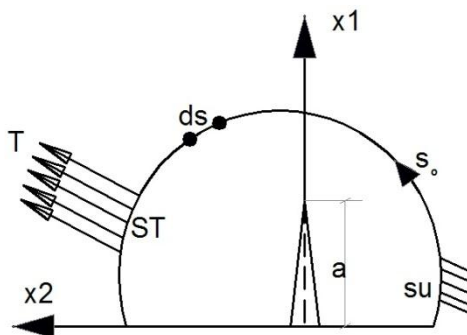


Figure 4. A planer cracked non linear elastic body with a boundary defined by S. ST and Su represent regions where the traction and displacement along the boundary are defined, **Saxena, 1998.**

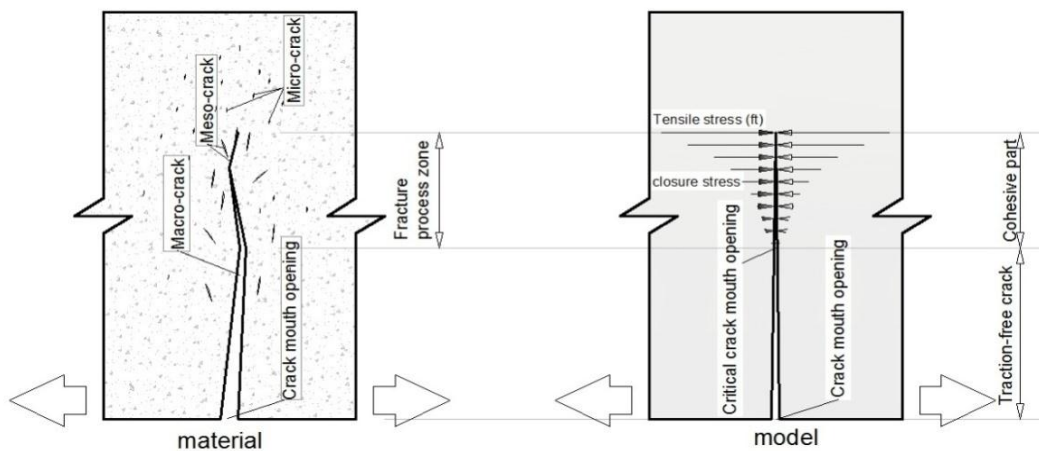


Figure 5. Crack scale in asphalt concrete material, Uzan and Levenberg, 2001.

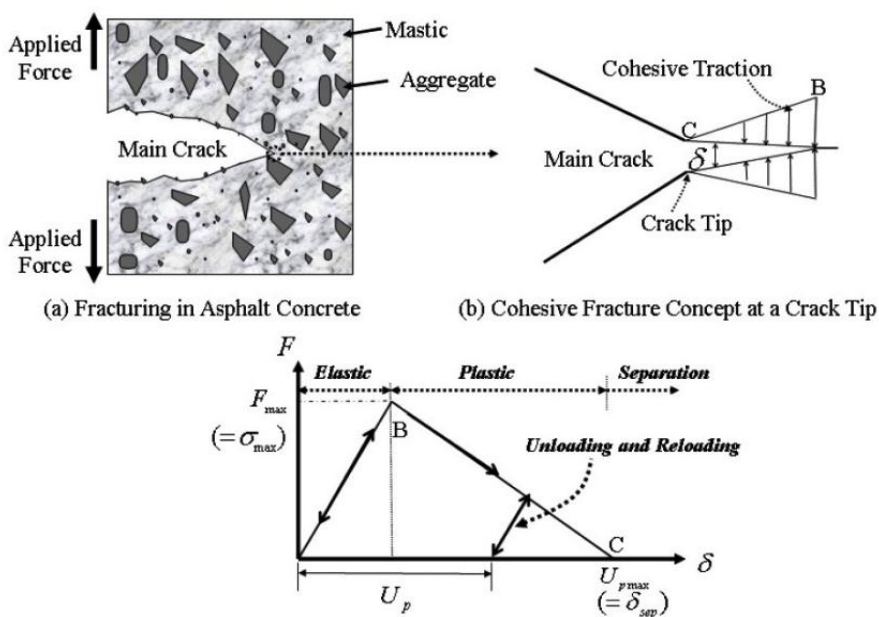


Figure 6. The schematic concept of bilinear cohesive softening model, Kim, H., et. al., 2008.

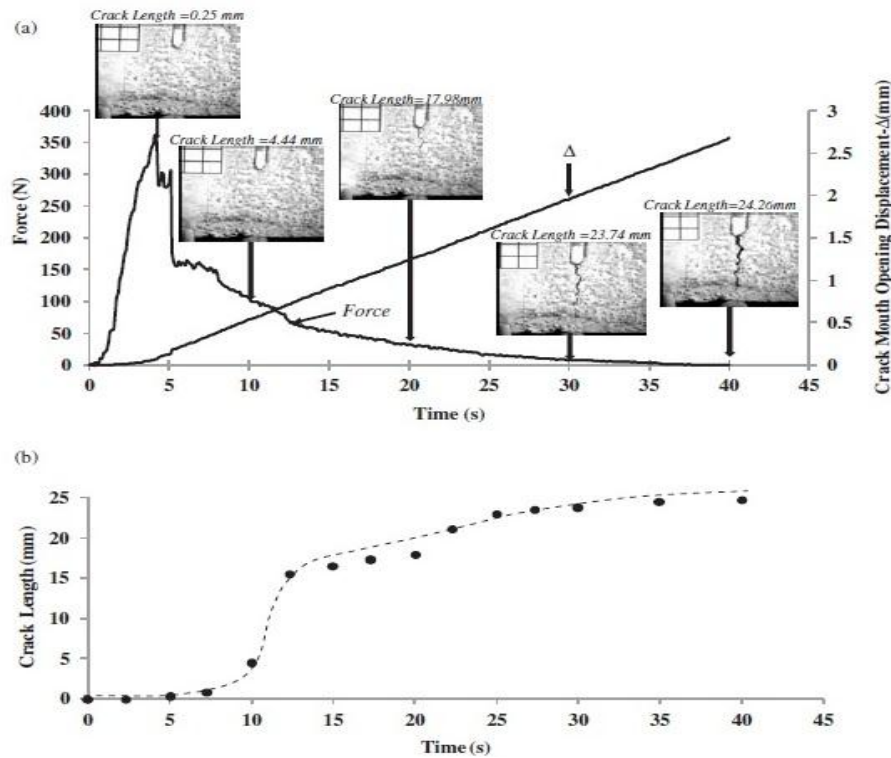


Figure 7. Typical load line displacement curve for tested beam sample at -20°C with displacement rate of 0.05mm/sec, Portillo and Cebon, 2008.

Table 2. Asphalt cements physical properties

Test	Test Conditions	ASTM, Designation (2010)	Units	Asphalt Cement		*SCRB criteria (2003)	
				40-50	60-70		
Penetration	100 ^{gm} , 25 °C, 5sec., 0.1 mm	ASTM D5	1/10 ^{mm}	47	64	40-50	60-70
Rotational Viscosity	135°C	ASTM D4402	Pas.sec	0.4625	0.353	---	---
	165 °C			0.125	0.113	---	---
Specific Gravity	25 °C	ASTM D70	----	1.04	1.03	---	---
Ductility	25 °C, 5 ^{cm} /min	ASTM D113	cm	>100	>100	>100	>100
Flash Point	-----	ASTM D92	°C	287	270	>232	>232
Solubility in trichloroethylene	-----	ASTM D2042	% wt	99.5	99.6	> 99	> 99
% Loss After Thin Film Oven Test	5hr @ 163°C, 50 ^{gm}	ASTM D1754	% wt	0.30	0.33	<0.75	<0.75
% from origin Penetration after Thin Film Oven Test	100 ^{gm} , 25°C, 5sec., 0.1 mm	ASTM D5	%	60	64	>55%	>52%
Ductility after Thin Film Oven Test	25 °C, 5 ^{cm} /min	ASTM D113	cm	75	>100	>25	>50

*SCRB: State Corporation for Roads and Bridges

**Table 3.** Physical properties of coarse and fine aggregates of AL Nebai quarry.

Property	ASTM Test Designation (2010)	Coarse Aggregate	Fine Aggregate	SCRB Specification (2003)
<i>Bulk Specific Gravity</i>	<i>C-127 and C-128</i>	2.610	2.630	
<i>Apparent Specific Gravity</i>	<i>C-127 and C-128</i>	2.690	2.708	
<i>Percent Water Absorption</i>	<i>C-127 and C-128</i>	0.464	0.715	
<i>Percent Wear (Los Angeles Abrasion)</i>	<i>C-131</i>	22.00	-----	<i>30 max</i>
<i>Soundness loss by sodium sulfate solution, %</i>	<i>C-88</i>	3.55	-----	<i>10 max</i>
<i>Fractured pieces, %</i>	-----	96	-----	<i>95 min</i>
<i>Sand Equivalent, %</i>	<i>D-2419</i>	-----	53	<i>45 min.</i>

Table 4. Chemical composition of AL-Nebai quarry aggregates.

Mineral Composition	% content
<i>Quartz</i>	80
<i>Calcite</i>	11
<i>Total Soluble Salts TSS</i>	2.0
<i>Gypsum</i>	0.45
<i>Organic Matter</i>	0.50

Table 5. Mineral composition of AL-Nebai quarry aggregates.

Chemical compound	% content
<i>Silica SiO₂</i>	82.52
<i>Lime CaO</i>	5.37
<i>Magnesia MgO</i>	0.78
<i>Alumina Al₂O₃</i>	0.48
<i>Ferric Oxide Fe₂O₃</i>	0.70
<i>Sulfuric Anhydride SO₃</i>	2.7
<i>Loss on Ignition</i>	6.55
<i>Total</i>	99.10



Table 6. Physical properties of mineral filler.

<i>Property</i>	<i>Test Result</i>
<i>Specific Gravity</i>	<i>2.720</i>
<i>Passing Sieve No.200 (0.075 mm)</i>	<i>95%</i>

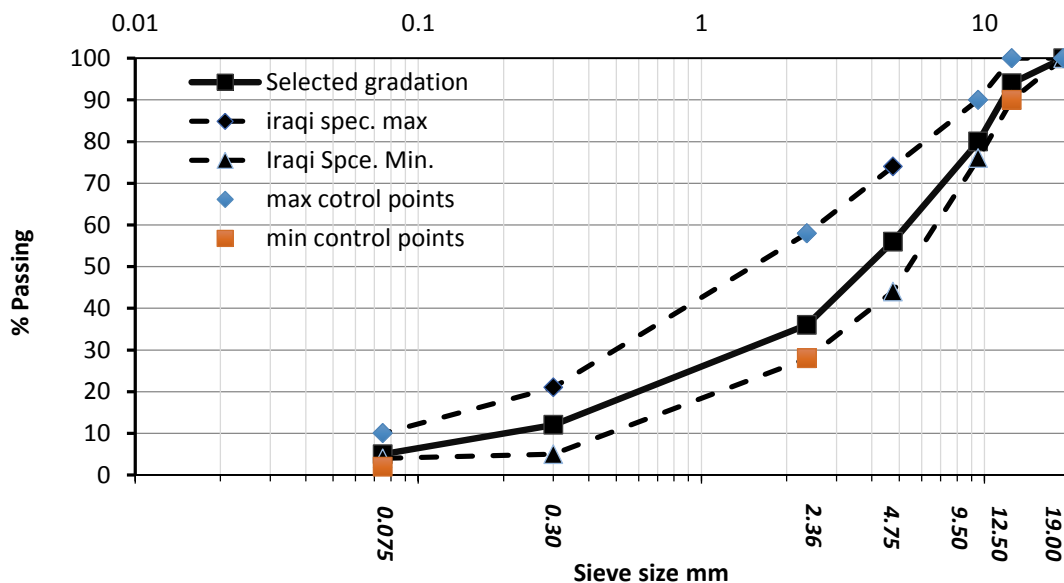


Figure 8. Selected aggregates gradation.

Table 7. Mixing and compaction temperatures for asphalt binder penetration graded.

Asphalt Binder Penetration Graded	Temperature °C	
	Mixing temperature	Compaction temperature
(40-50)	158	148
(60-70)	153	142

Table 8. SUPERPAVE gyration levels design ,SP-2, 2003.

ESALs (millions)	Number of Gyration		
	N initial	N design	N max
<0.3	6	50	75
0.3 to 3.0	7	75	115
3.0 to 30.0	8	100	160
≥ 30.0	9	125	205

Table 9. HMA volumetric properties of wearing mix at OBC ,SP-2, 2003.

Mix Property	Optimum Binder Content 4.70%	SUPERPAVE Criteria
Air voids	4.00%	4.00%
VMA	15.10%	Min. 14%
VFA	73.25%	65%-75%
G_{mb}/G_{mm} @ $N_{initial}$ 8	85.10%	Max. 89%
G_{mb}/G_{mm} @ N_{design} 100	96.00%	96.00%
G_{mb}/G_{mm} @ $N_{maximum}$ 160	96.742%	Max. 98%



Plate 1. Optimum binder content determination using SUPERPAVE requirements.

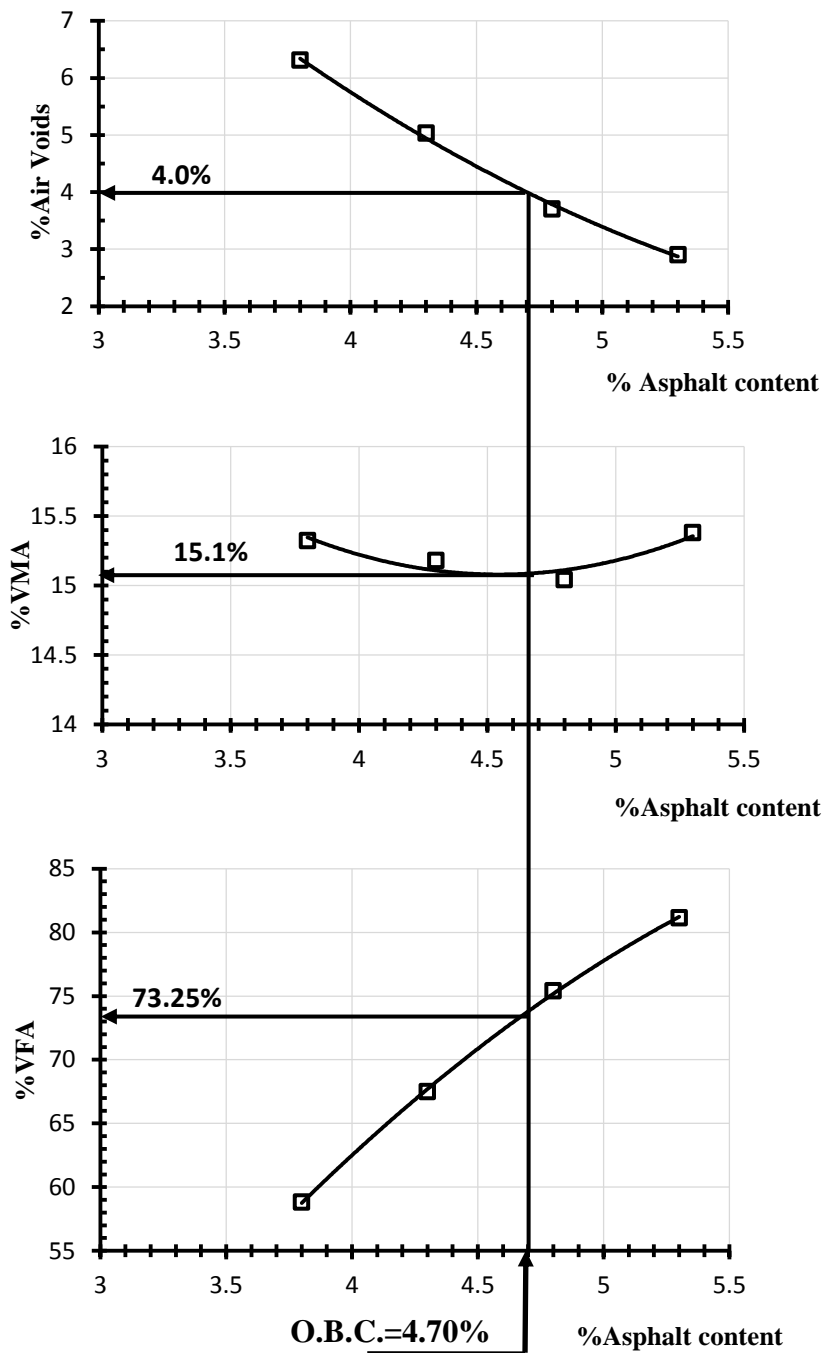


Figure 9. OBC determination for wearing layer according to SUPERPAVE criteria.



Plate 2. Beams specimens preparation.

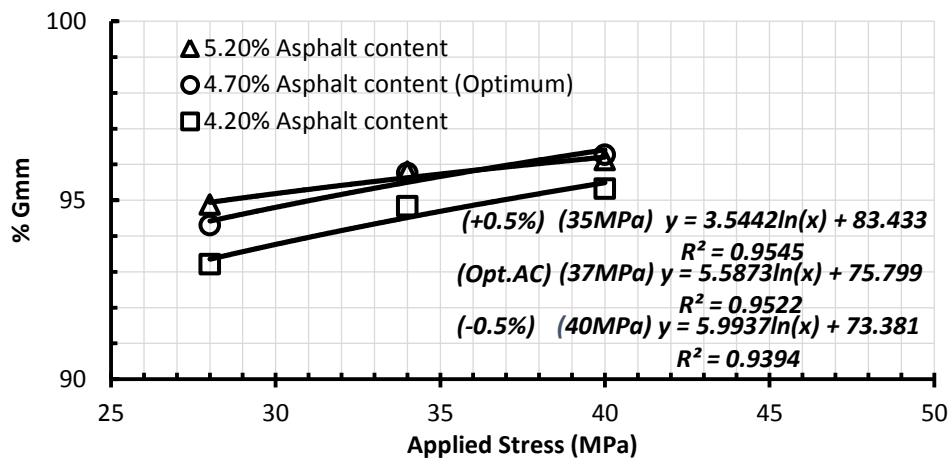


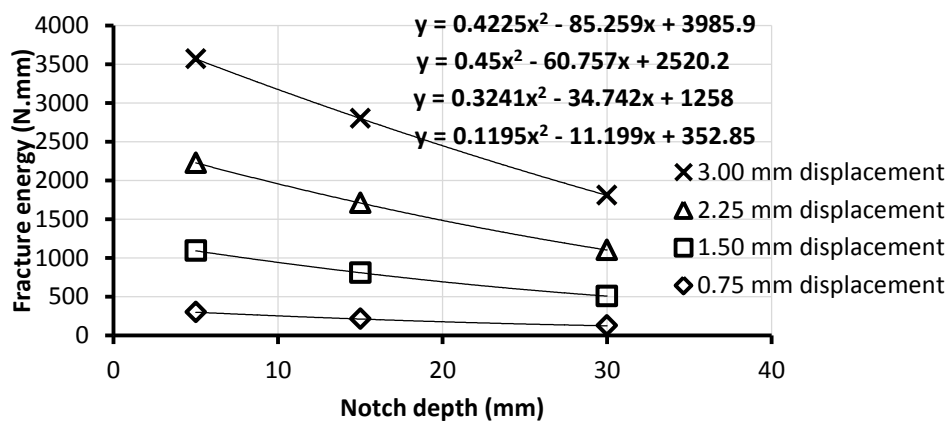
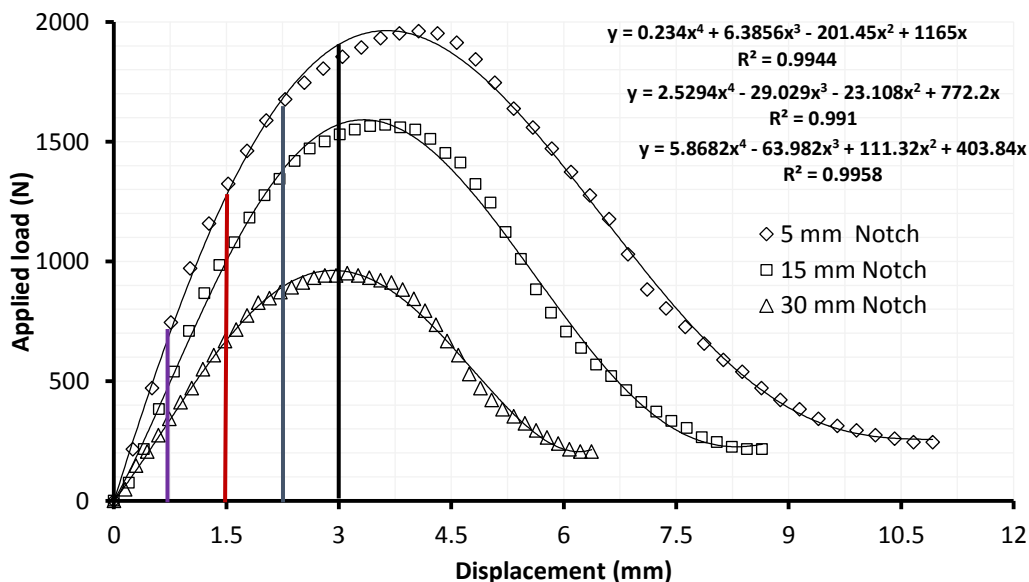
Figure 10. Applied stress and %G_{mm} relations for beams specimens with different asphalt content.

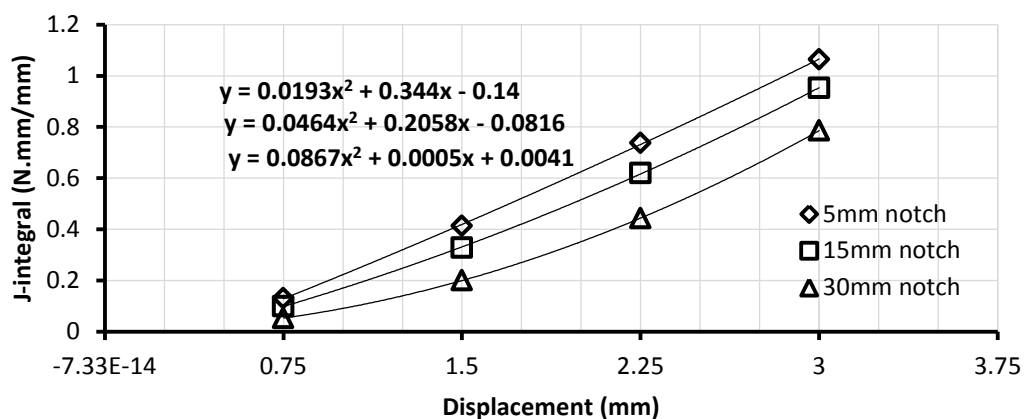


Plate 3. Steel plates arrangements which used for making notches.

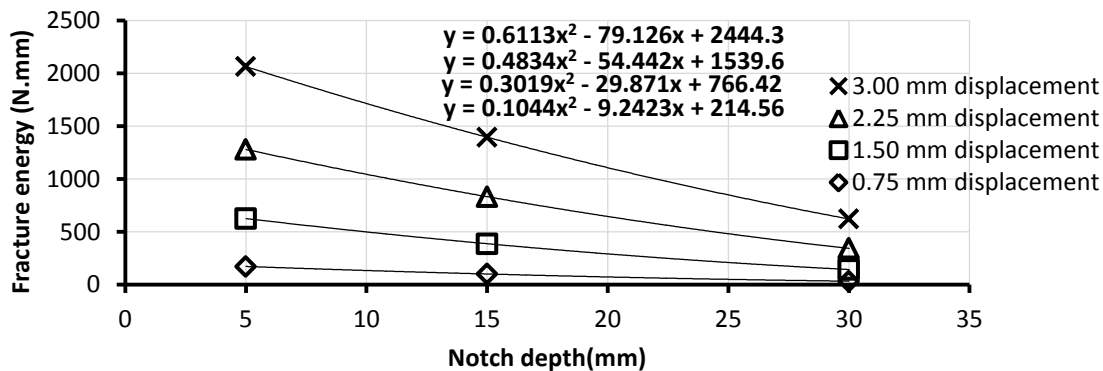
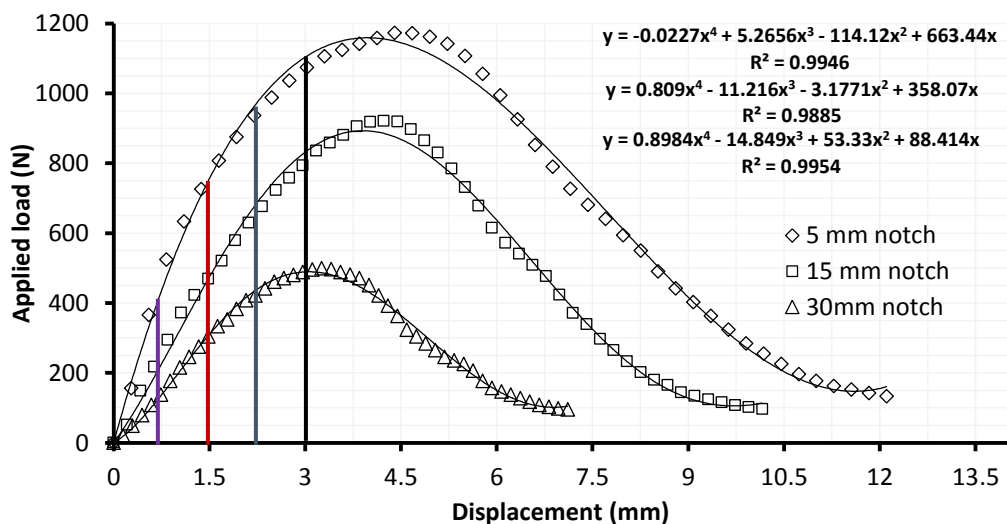


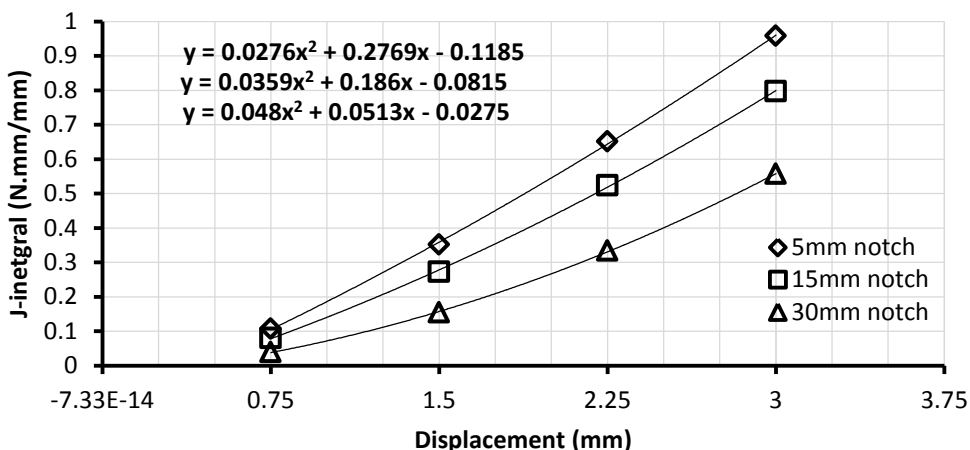
Plate 4. Load frame device of multi deformations rates and tested specimens.





Figures 11-a, b, and c. Estimating fracture properties, in-terms of (U) fracture energy and J-integral for beams specimens with different notch depths tested with 3-point BBT at 20±1°C.





Figures 12-a, b, and c. Estimating fracture properties, in-terms of (U) fracture energy and J-integral for beams specimens with different notches depths tested with 3-point BBT at 30±1°C.

Table 10. Calibration function $F(a/W)$ magnitude for studied notch depth.

Notch depths	5 ^{mm}	15 ^{mm}	30 ^{mm}
$F(a/W)$	2.836	4.981	10.107

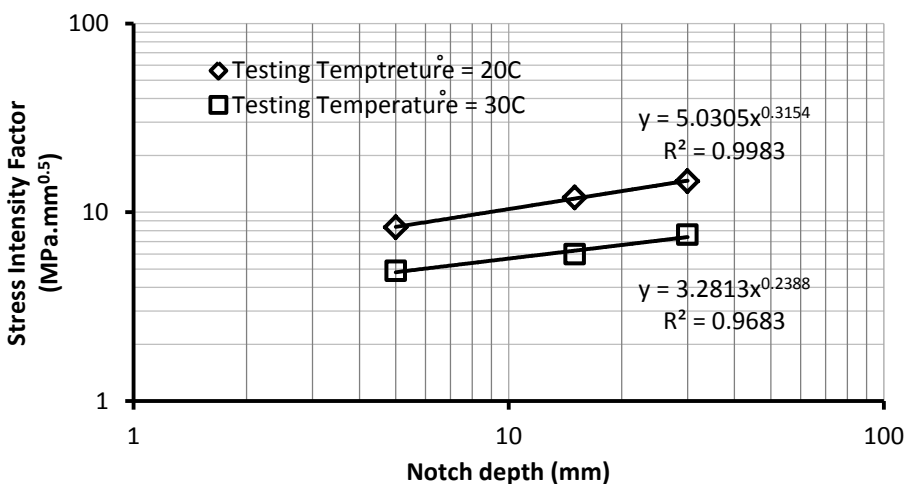


Figure 13. Stress Intensity Factor (K) for beams specimens of different notch depth tested monotonically at 20±1°C and 30±1°C.

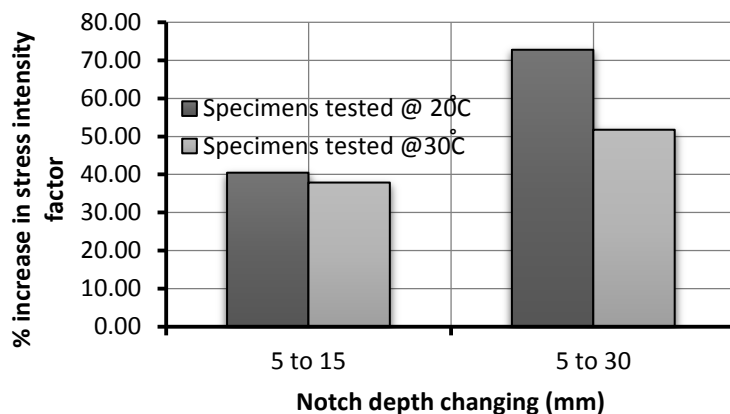


Figure 14. Percentage increase in stress intensity factor with increasing notch depth for beam specimens tested at $20\pm 1^\circ\text{C}$ and $30\pm 1^\circ\text{C}$ with different notch depths.

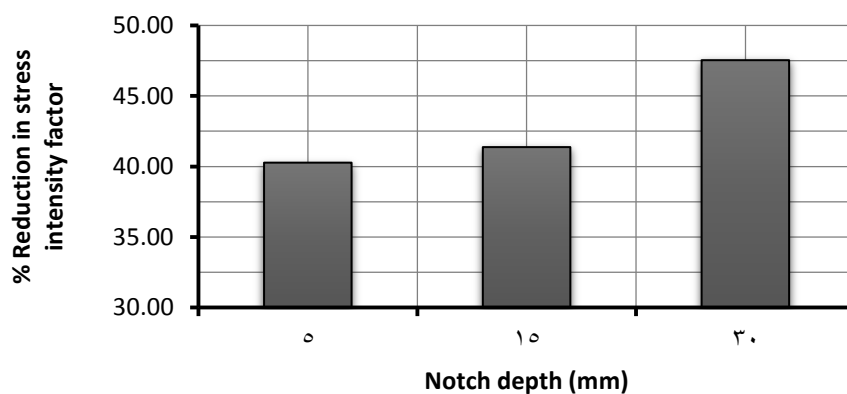


Figure 15. Percentage drop in stress intensity factor with increasing testing temperature for beam specimens tested at $20\pm 1^\circ\text{C}$ and $30\pm 1^\circ\text{C}$ with different notch depths.

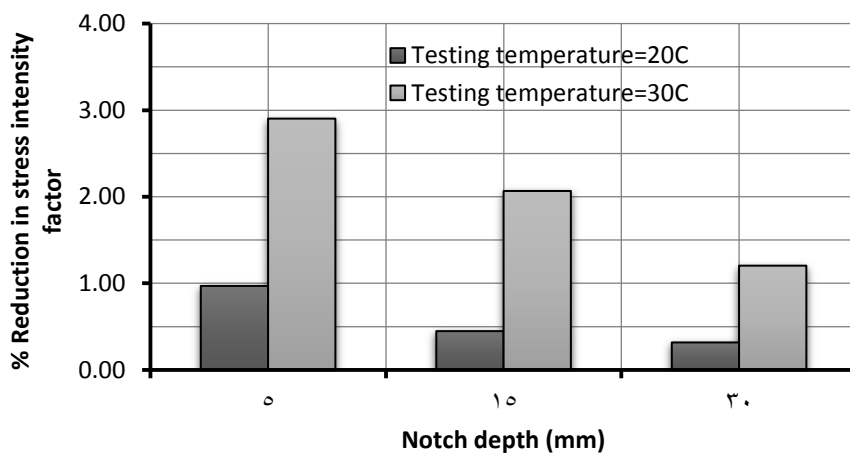


Figure 16. Percentage reduction in stress intensity factor for beam specimens tested at $20\pm 1^\circ\text{C}$ and $30\pm 1^\circ\text{C}$ with different notch depths due to change the asphalt type.

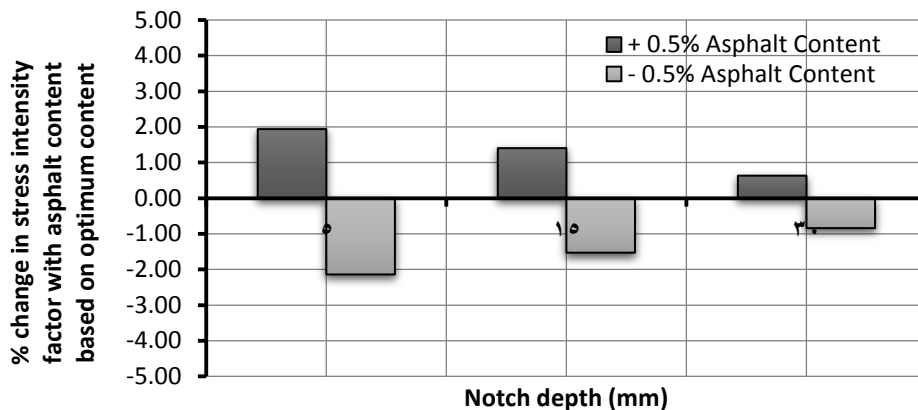


Figure 17. Percentage of change in stress intensity factor for beams specimens tested at 20±1°C with notch depths.

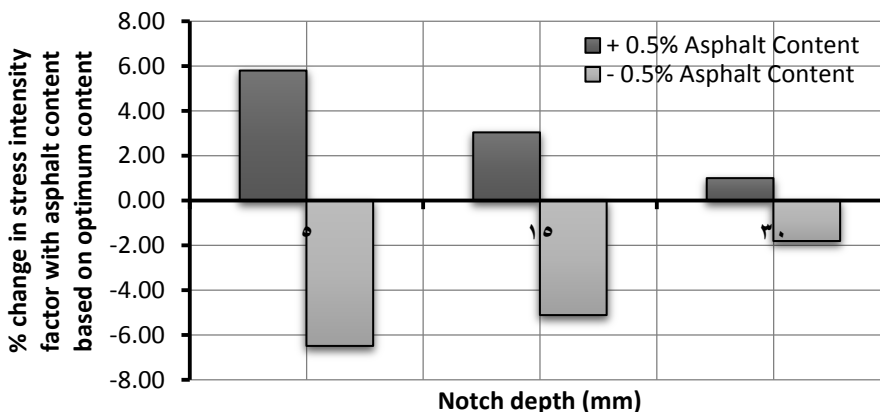


Figure 18. Percentage of change in stress intensity factor for beams specimens tested at 30±1°C with notch depths.

Table 11. Stress intensity factor sensitivity according to study parameters.

Parameters	Percentage Effect	Sensitivity
Testing Temperature	>40%	Relatively High
Notch depth	>40%	Relatively High
Asphalt Content	<6%	Relatively low
Asphalt Type	<3%	Relatively low